coatings

MDPI

Article

Wavelength-Selective Coatings on Glass with High Hardness and Damage Resistance

Karl W. Koch [1], Lin Lin [1], James J. Price [1], Chang-Gyu Kim [2], Dong-Gun Moon [2], Sang-Yoon Oh [2], Jung-Keun Oh [2], Jeong-Hong Oh [2], Charles A. Paulson [1], Binwei Zhang [1], Ananth Subramanian [1], Alexandre Mayolet [1], Carlo Kosik Williams [1] and Shandon D. Hart [1,*]

[1] Corning Incorporated, Corning, NY 14831, USA; kochkw@corning.com (K.W.K.); linl2@corning.com (L.L.); pricejj@corning.com (J.J.P.); paulsonca@corning.com (C.A.P.); zhangb4@corning.com (B.Z.); subramana@corning.com (A.S.); mayoleta@corning.com (A.M.); kosikwilca@corning.com (C.K.W.)

[2] Corning Incorporated, Asan-si, Chungcheongnam-do 336-725, Korea; changgyu.kim@corning.com (C.-G.K.); donggun.moon@corning.com (D.-G.M.); sangyoon.oh@corning.com (S.-Y.O.); jungkeun.oh@corning.com (J.-K.O.); jeonghong.oh@corning.com (J.-H.O.)

* Correspondence: hartsd@corning.com

Received: 23 October 2020; Accepted: 11 December 2020; Published: 17 December 2020

Abstract: Wavelength-selective coatings are broadly applied across diverse industries such as solar energy management, infrared sensing, telecommunications, laser optics, and eye-protective lenses. These coatings have historically not been optimized for hardness or mechanical durability and typically suffer from higher susceptibility to scratch and damage events than uncoated glass. In this work, we describe a family of wavelength-selective coatings with hardness and scratch resistance that are significantly higher than the chemically strengthened glass substrates on which the coatings are fabricated. The coatings are made using industrially scalable reactive sputtering methods. Wavelength-selective coatings are fabricated with nanoindentation hardness as high as 16–20 GPa over indentation depths ranging from 200 to 800 nm, as well as excellent durability in aggressive scratch testing. Tunable visible to near-infrared wavelength selectivity ratios (reflectance of stopband: reflectance of passband) as high as 7:1 are achieved. The feasibility of narrowband hard coating design is also demonstrated, with visible narrowband transmission having a peak FWHM of ~8 nm (~1.6%). A unique "buried layers" hard coating design strategy is shown to deliver particularly excellent hardness profiles. These designs can be tailored for a variety of different wavelengths and selectivity ratios, enabling new uses of wavelength-selective optics in mechanically demanding applications.

Keywords: wavelength; selective; coating; hardness; color; optical; interference; scratch; damage

1. Introduction

Optical interference coatings utilize the physics of thin-film interference [1–4] to create unique optical properties that cannot be achieved using typical bulk materials. These coatings have been studied and applied for a wide variety of uses, including low reflection optics [4,5], high reflection mirrors [6–8], solar energy management [9], telecommunications [10], infrared (IR) sensors [11,12] and more. Despite this broad design flexibility and utility, optical interference coatings have historically suffered from relatively low scratch or damage resistance, especially when compared to modern chemically strengthened glasses, such as Corning Gorilla Glass®. This relatively low durability remains true even for coatings using thin layers of materials that can have high hardness, such as silicon nitride [13,14], because the design of these coatings relies on layers that are too thin (~0.1 micron or less) to protect the coating or the underlying substrate against common scratches in these types of applications. Through extensive analysis of used consumer electronics devices with chemically strengthened glass

enclosures, we found that 70–80% of surface scratches were single-event "micro-ductile" [15] scratches with depths in the range of about 0.1–1 micron. These types of scratch events are too deep and severe for a typical thin-film interference coating to withstand, regardless of the materials employed in the coating. Recently, we demonstrated a new optomechanical design approach, which dramatically boosted the hardness and practical scratch resistance of anti-reflection (AR) coatings [16]. Versions of these high-hardness AR coatings have already been deployed on millions of consumer electronics devices with excellent manufacturing and field performance; these coatings have also been shown to improve electronic display readability and enable reduced display energy consumption [17]. In this current work, we show that, by expanding on the design principles of [16], we can create tunable wavelength-selective optical coatings that have very high levels of hardness and outstanding resistance to aggressive scratch testing. We demonstrate tunable broadband wavelength selectivity in the visible to near-infrared (NIR) wavelength range, as well as the feasibility of narrowband optical transmission. Coatings using a unique "buried layers" design demonstrate especially high nanoindentation hardness of 16–20 GPa at indentation depths of 200–800 nm, as well as excellent practical scratch resistance. These demonstrations pave the way for new applications of wavelength-selective optics in mechanically demanding fields, potentially including IR/UV/visible solar reflectors; colored or color-shifting films for security, smartphone, ophthalmic, or automotive applications; and IR bandpass filters for sensor applications.

2. Materials and Methods

Wavelength-selective, high-hardness coatings were designed using optical transfer matrix simulations [1], incorporating optical properties measured by spectroscopic ellipsometry for the experimentally fabricated coating materials. Coatings were made using reactive sputtering deposition processes [18–24]. These sputtering fabrication processes have been found to deliver desirable combinations of coating density, stress, hardness, optical absorption, layer thickness control, and deposition rates, enabling the efficient manufacturing of such coatings. Exemplary multilayer coatings are comprised of high hardness, high refractive index materials, such as SiN_x, SiO_xN_y, AlO_xN_y, or $SiAluO_xN_y$, layered with a low-index material, such as SiO_2 (see Appendix A for detailed example coating designs). In this work, metallic aluminum or silicon sputtering targets were combined with non-reactive argon and reactive oxygen and nitrogen process gases in a sputtering chamber. For each coating material and sputtering process, a recipe development specific to each coating chamber geometry was needed to achieve the desired targets of low optical extinction coefficient ($k < 0.001$ at 400 nm wavelength), high material hardness (>18 GPa for a single-material, 2-micron thick layer), and low or controlled film stress (0–400 MPa compressive). In order to achieve high hardness levels using SiN_x, SiO_xN_y, AlO_xN_y, or $SiAluO_xN_y$ materials, film compositions may include between 0 and 20 atom% oxygen and 30 and 50 atom% nitrogen, with resulting refractive indices in the range of 1.9–2.1. For example, high hardness, high optical transparency SiO_xN_y film materials can be deposited by reactive magnetron sputtering from a silicon target [18,19]. Using a laboratory deposition chamber (ATC-2200 with A330-XP UHV magnetron sputtering source from AJA International (N. Scituate, MA, USA) with 3" sputtering targets, example process conditions for SiO_xN_y deposition on glass substrates included 400 W RF power to the Si target supplied at 13.56 MHz, 30 sccm Ar gas flow, 40 sccm N_2 gas flow, 0.4 sccm O_2 gas flow, 1.5 mTorr process pressure, and a deposition temperature of 100–200 °C. These process conditions led to SiO_xN_y film materials with a refractive index of ~1.9 and measured hardness of >17 GPa, with a corresponding composition of ~48 atom% Si, 10 atom% O, and 42 atom% N. Using a similar process with O_2 gas flow set to zero, SiN_x or SiO_xN_y materials with only trace amounts of oxygen were deposited with a refractive index >2.0 and measured hardness >20 GPa. For films in this range of hardness, typical elastic modulus values were in the range of 200–240 GPa, resulting in H/E ratios of ~0.8. These high-index, high-hardness materials were layered with a low-index material such as SiO_2 to achieve the optical interference effects targeted and designed through the transfer matrix simulations. It is necessary to have a low-index material component of the

coating to achieve the desired wavelength selectivity, and materials with low refractive index typically have lower hardness (due to the relationship of both hardness and refractive index to electron and bonding density in the materials). Lower-index, lower-hardness SiO_2 films can be made using similar deposition processes as those described above for SiN_x and SiO_xN_y, replacing N_2 gas flow with O_2 gas flow only. All coated samples, as well as the chemically strengthened glasses without hard coatings used for comparison, included a very thin (<10 nm) oleophobic fluorosilane layer on the top-most user-facing surface. These coatings are common on glasses in consumer electronics applications and tend to reduce the friction of the surface without having a significant effect on optics or hardness.

We performed optical reflection and transmission spectroscopy using an Agilent Cary 5000 UV-Vis-NIR spectrophotometer (Santa Clara, CA, USA) recording spectra with 2 nm wavelength step size and 4 nm resolution. The spectra were used to determine CIE L*a*b* color coordinates and perform reverse engineering of the designs. In addition, we used a Woollam M-2000 variable-angle spectroscopic ellipsometer, varying the input angle of the measurement from 45° to 80° and scanning the wavelength from 250 to 1680 nm. These measurements were used to determine single-layer film material dispersion and deposition rates for individual processes, as well as to reverse-engineer refractive index and thickness for film stacks consisting of multiple layers.

Coating hardness was measured via nanoindentation using a Berkovich diamond tip on a KLA Instruments G200 Nano Indenter (Milpitas, CA, USA). To extract hardness, we followed the widely accepted Oliver–Pharr approach [25,26], combined with a special technique known as the continuous stiffness mode [27]. The continuous stiffness mode superimposed a small (+/−1 nm) oscillatory signal at 52 Hz during the loading cycle, which enabled hardness to be measured continuously as a function of indentation depth. Hardness measurements were typically carried out with 10 replicates to depths of 500–1000 nm, with typical standard deviations of 0.3–0.5 GPa. An aggressive "garnet scratch test" was employed on Design Strategy 2 samples consisting of a single pass with a 150 grit garnet sandpaper swatch, with either 1 or 4 kg applied load over a ~0.6 cm × 0.6 cm contact area. The samples were visually graded with the naked eye after this test, with Grade A = no visible scratches; B = 1 visible scratch; C = 2 visible scratches; and D = 3 or more visible scratches. This garnet scratch test has been found to produce scratches of a similar depth and severity as customer field returns showing heavy damage from the consumer electronics industry.

The optomechanical design strategy used to create high-hardness wavelength selective coatings was related to our recently published approach to create high-hardness antireflective coatings [16]. In short, the coating layer structure was conceptually divided into one or more optical interference layer regions, which performed the desired optical functions, and one or more hard coat layer regions, which provided high hardness at depths that were typical of real-world scratch events. In many cases, the same material can be used for both the hard coat region and the high-index component of the optical interference layer regions, while a softer low-index material is needed in the layered regions to create the desired optical interference effects. For antireflective coatings, multiple interference layer regions are employed to lower reflectance; in the case of wavelength-selective coatings, one or more interference layer regions is employed to achieve wavelength-selective reflectance, and one or more layers may provide antireflective function as well. These antireflective layer regions are used to control optical resonances (rapid oscillations in reflectance and transmittance) generated by the reflecting wavelength-selective layers and also enable the varying thickness of the hard coat layer with only a small impact on optical performance. Although the optical performance of thin films is typically highly sensitive to both the refractive index and thickness of each layer, the ability to substantially decouple optical performance from the thickness of the hard coat region for some designs is one of the unique features of this "modular" coating design approach [16].

3. Results

Wavelength selectivity was demonstrated through the fabrication of coatings with varying reflected visible colors (shown in Figure 1). Visible colors are especially apparent in reflectance when

the samples are viewed against a black background (top half of each sample image), while transmitted color (shown by the sample appearing against a white background in the bottom half of each sample image) typically appears more neutral in these designs due to their relatively high average transmission. The choice of visible color wavelength selectivity allows direct human observation of the high coating uniformity of the wavelength-selective interference effects, as well as human eye ranking of the effects of scratches on optical performance. Beyond the visible color demonstrations shown here, these coatings can also be designed for IR and UV shielding or selectivity.

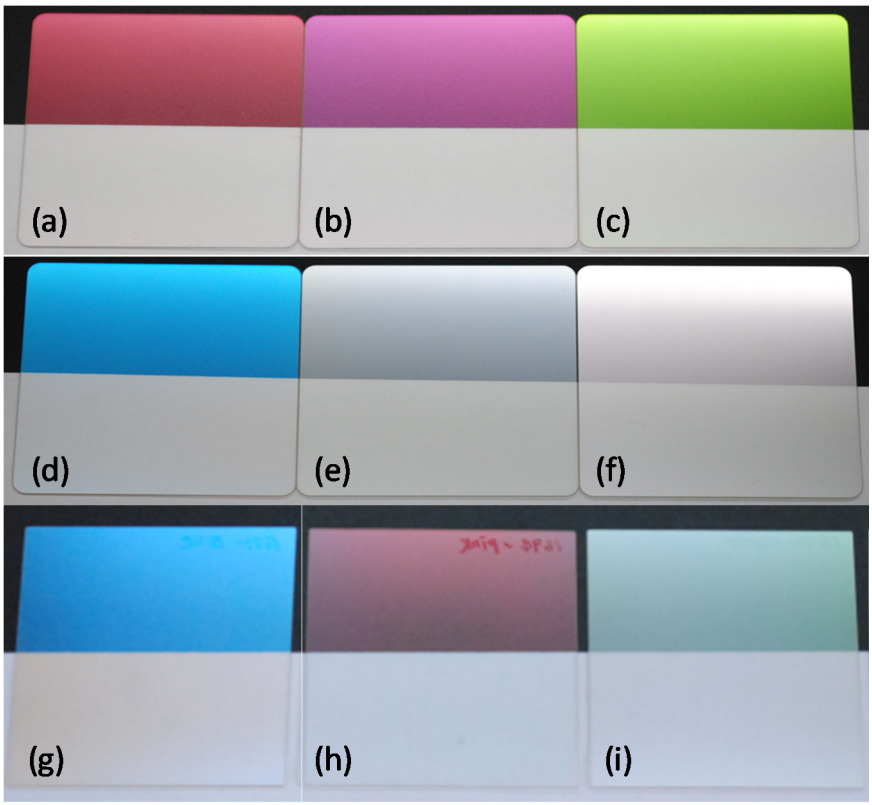

Figure 1. Optical images of experimental glass samples having wavelength-selective hard coatings. Samples are arranged with a black background underneath the top half of each sample and a white background under the bottom half of each sample. Vivid colors are visible in reflectance against a black background, while transmitted light viewed against the white background has relatively more neutral colors in these designs. Samples (**a**–**e**) represent coating Design Strategy 1, where the wavelength-selective interference layers are located above the thickest hard coating layer; samples (**f**–**i**) represent Design Strategy 2, where the wavelength-selective layers are "buried" below this hard coat layer. Samples are named as (**a**) WSC-Red-1, (**b**) WSC-Pink-1, (**c**) WSC-Green-1, (**d**) WSC-Blue-1, (**e**) WSC-Silver-1, (**f**) WSC-Silver-2-B, (**g**) WSC-Blue-2-B, (**h**) WSC-Pink-2-B, and (**i**) WSC-Silver-3-B.

Two distinct coating design approaches were tested in this work, resulting in two distinct groups of coated samples. Design Strategy 1 places optical interference layers, which generate the wavelength-selective response, on the user-facing side of the thickest hard coating layer in the multilayer coating stack, while buried antireflective layers (also named "impedance-matching layers" in [16]) are below this hard coat layer. Samples (a) through (e) in Figure 1 are designed and fabricated using Design Strategy 1. Samples (f) through (i) in Figure 1 are designed and made using Design Strategy 2, which places the wavelength-selective optical interference layers below the thickest hard coating layer and a single antireflective layer on the user-facing side of this hard coat layer. Design Strategy 2 can be said to employ a "buried active layers" design approach since the layers imparting most of the targeted optical functions are buried below a thick hard coating layer. Detailed coating designs for Design

Strategy 1 are contrasted with Design Strategy 2 in Appendix A. The purpose of the buried antireflective layers in Design Strategy 1 is to minimize oscillations in the reflectance and transmittance spectra and to allow flexible thickness changes to the thickest hard coating layer (layer 7 in Design Strategy 1 samples, see Appendix A). The ability to change the thickness of the thickest hard coating layer without dramatically impacting the optics of the entire coating system is one of the unique features of this "modular" coating design approach and is due to the presence of these buried antireflective layers. In contrast, Design Strategy 2 utilizes buried wavelength-selective layers and a single exposed antireflective layer on the user-facing side of the thickest hard coating layer, which also aids in the control of reflectance and transmittance oscillations. Observed differences in performance between Design Strategy 1 and 2 are further described below.

3.1. Design Strategy 1: Buried Antireflective Layers, Exposed Wavelength-Selective Layers

As shown in Figure 2, the wavelength-selective nature of these coatings is broadly tunable and can be tailored for a variety of end-use applications. The optical interference nature and low absorbance of these coatings result in transmittance values that are very close to (100%—reflectance). These reflectance and transmittance spectra show a low degree of oscillation or ripple, which is related to the presence of the buried antireflective layers that effectively eliminate reflectance at the interface between the glass substrate and the thick hard coating layer, despite a large difference in refractive index between the glass and the thick hard coating layer. These buried antireflective layers also allow tailoring of the thickness of the thick hard coating layer with minimal effect on optical performance, as demonstrated in [16]. Wavelength selectivity ratios (reflectance of stopband: reflectance of passband) of up to 5:1 are demonstrated in this sample set. These selectivity ratios can be enhanced even more with further design optimization, potentially requiring more layers. These designs can also be readily modified for operation in UV or IR wavelength ranges.

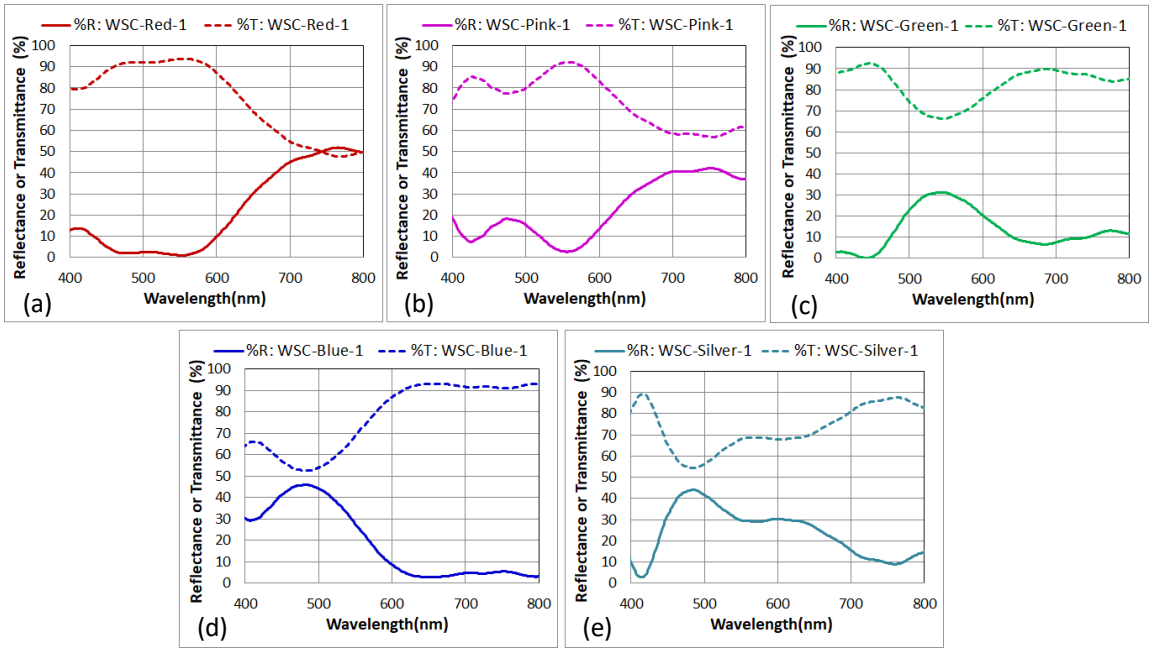

Figure 2. Reflectance (8 degrees light incidence) and Transmittance (0 degrees) for Design Strategy 1 wavelength-selective hard coatings: (**a**) WSC-Red-1, (**b**) WSC-Pink-1, (**c**) WSC-Green-1, (**d**) WSC-Blue-1, and (**e**) WSC-Silver-1. Wavelength selectivity is broadly tunable across the visible to near IR spectrum through interference layer design.

Figure 3 and Table 1 summarize the apparent hardness vs. indentation depth for the five Design Strategy 1 coatings tested. Variations in coating design, in particular, the amount of lower-hardness

SiO_2 material coated above the thickest hard coat layer, lead to varying levels of hardness vs. depth (see Appendix A for detailed coating structures). For comparison, the hardness measured by this method of typical chemically strengthened glass without coatings is approximately ~8 GPa. The higher hardness of sample WSC-Pink-1, can be understood from its coating structure relative to the other designs. Sample WSC-Pink-1 has a higher fraction of high-hardness SiN_x material on the user-facing side (233 nm SiN_x out of 421 nm total in layers 8 through 12) above the thickest hard coating layer (layer 7). Sample WSC–Blue–1, has the lowest apparent hardness and the lowest fraction of SiN_x material (89 nm of SiN_x out of 465 nm total in layers 8 through 12). The measured hardness of these coatings depends on the interaction of the indenter tip with the mechanical response of multiple layers simultaneously [28], which can be described as an interaction volume effect.

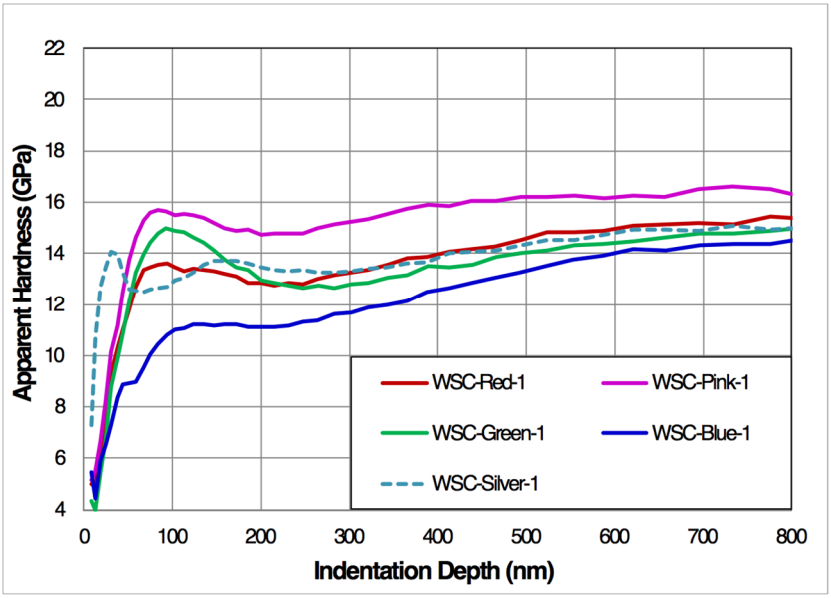

Figure 3. Measured nanoindentation hardness vs. indentation depth for Design Strategy 1 hard coatings. Variations in hardness are due to the thickness and the number of layers that are included in the design to achieve the targeted wavelength selectivity.

Table 1. Summary of key mechanical properties for Design Strategy 1 hard coatings.

Sample	Hardness at 100 nm GPa	Hardness at 500 nm GPa
WSC-Red-1	13.5	14.5
WSC-Pink-1	15.5	16.2
WSC-Green-1	14.9	14.0
WSC-Blue-1	11.0	13.3
WSC-Silver-1	12.9	14.3

3.2. Design Strategy 2: Buried Wavelength-Selective Layers, Single Exposed Antireflective Layer

In order to maximize the hardness of wavelength-selective coatings to an even greater extent, Design Strategy 2 employs wavelength-selective interference layers that are buried below a thick (~2 micron) hard coating layer, together with a single air-side SiO_2 layer providing some level of anti-reflection at the user-facing air-side interface which helps to control oscillations in reflectance and transmittance. Using this "buried active layers" approach, we were able to design coatings with very high hardness in the range of 16–20 GPa over indentation depths ranging from 200 to 800 nm (more than double that of typical chemically strengthened glass). The optical response of the coatings is illustrated

in Figures 4 and 5, demonstrating a tunable visible color wavelength response comparable to the set of Design Strategy 1 samples above. This tuning can also be extended into non-visible wavelength ranges, as demonstrated by the reflectance stopband extending into the near-IR wavelength range for sample WSC-Pink-2-B.

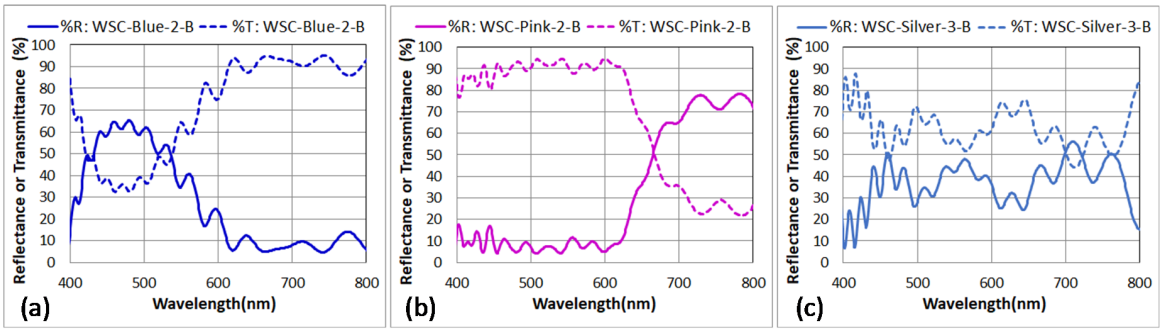

Figure 4. Reflectance (8 degrees light incidence) and transmittance (0 degrees) for Design Strategy 2 hard coating samples: (**a**) WSC-Blue-2-B, (**b**) WSC-Pink-2-B, and (**c**) WSC-Silver-3-B. Wavelength selectivity is broadly tunable through the interference layer design. High wavelength selectivity is demonstrated using Design Strategy 2, which uses buried interference layers to maximize hardness. A stopband passband reflectance ratio of >6:1 is demonstrated for (**a**) WSC-Blue-2-B and >7:1 for (**b**) WSC-Pink-2-B.

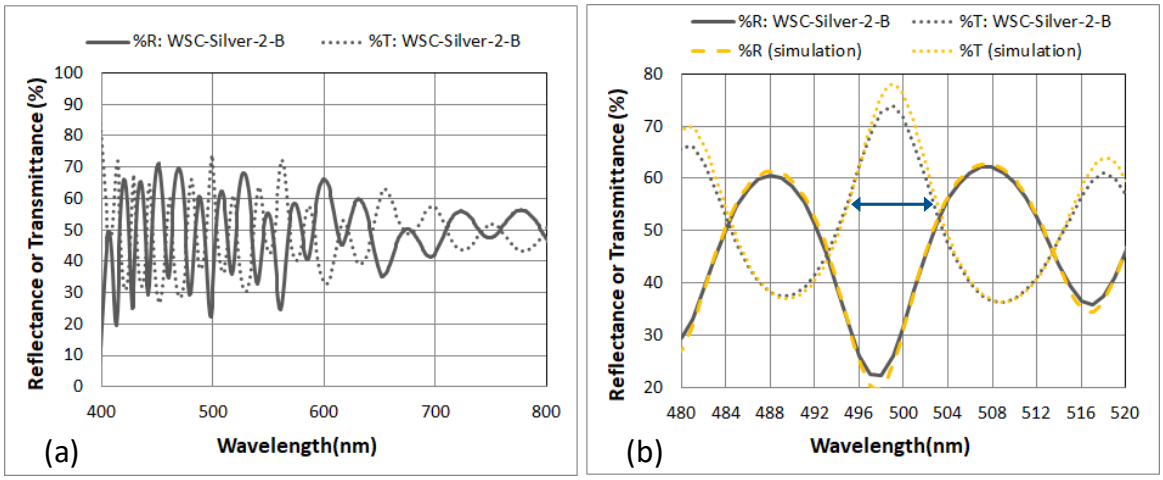

Figure 5. Reflectance and transmittance for wavelength selective hard coating sample (**a**) WSC–Silver–2–B and (**b**) WSC-Silver-2-B, narrowband detail view, made using Design Strategy 2. (**a**) shows multiple high-frequency oscillations in reflectance and transmittance, leading to narrowband features are observed in the WSC–Silver–2–B design. (**b**) shows narrowband optical transmission due to resonant cavity effects in this hard coating design, with the highlighted transmission peak having a FWHM of ~8 nm or ~1.6% of the central wavelength (blue arrow). Experimental results (grey) show good agreement with transfer matrix simulations (gold) for transmittance at 0 degrees and reflectance at 8 degrees. We expect that these designs can be further optimized for narrowband applications while preserving the high hardness coating structure.

In addition to the broadband wavelength selectivity illustrated in Figure 4, Figure 5 shows the feasibility of narrowband wavelength sensitivity in these hard coating designs. Although not optimized for narrowband transmission, the coating design WSC-Silver-2-B demonstrates a narrow passband of ~8 nm FWHM centered near 500 nm wavelength (~1.6% FWHM). The half-maximum level here is taken to be halfway between local maxima and minima. Figure 5b also demonstrates the close agreement

between transfer matrix simulations and experimental coating results. These hard coating designs can be further optimized for specific narrowband applications where high mechanical durability is desired.

The mechanical properties of Design Strategy 2 coatings are summarized in Figure 6 and Table 2, illustrating high coating hardness in the 200–800 nm depth range. The increased hardness over Design Strategy 1 is apparent and can be understood from the designs as related to having only a single antireflective SiO_2 layer placed above the thickest hard coating layer (see Appendix A). Design Strategy 2 also maximizes the use of the higher-hardness SiN_x material, which is measurably harder than the SiO_xN_y material used in some layers of the Design Strategy 1 coatings. The variations in hardness between the different Design Strategy 2 coatings summarized in Figure 6 and Table 2 can be seen to correlate with the thickness of the outermost SiO_2 layer. Sample WSC-Silver-2-B has the lowest apparent hardness of the Design Strategy 2 coatings, correlating with an outermost SiO_2 layer thickness of 133 nm above a ~2000 nm thick hard coat layer. Samples WSC-Blue-2-B and WSC–Silver-3-B have higher hardness profiles, and both have lower thicknesses of their outermost SiO_2 layer, 80 and 94 nm, respectively. Measured film stress levels are similar for both Design Strategy 1 and Design Strategy 2 coatings, being in the range from −50 to −200 MPa (compressive) for all example coatings shown from both design strategies.

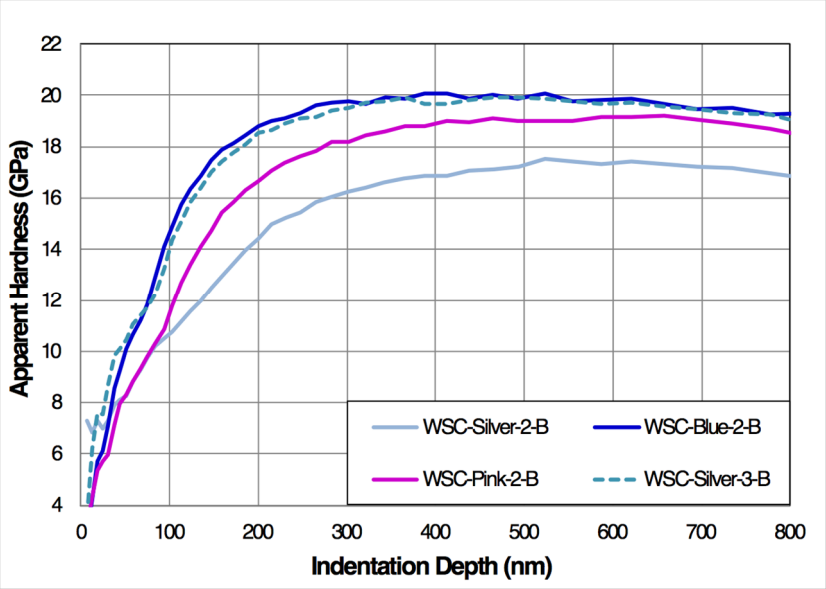

Figure 6. Measured nanoindentation hardness vs. indentation depth for Design Strategy 2 hard coatings. These designs use a "buried active layers" approach to maximize hardness in the 200–800 nm depth range, which leads to excellent scratch resistance.

High hardness has previously been shown to correlate with resistance to aggressive scratch testing [16]. To confirm this, we employed an aggressive garnet scratch test on the Design Strategy 2 samples. This test employed a 1–4 kg load on a 0.36 cm^2 garnet sandpaper swatch with a single scratching pass using a mechanical abrader instrument. All of the Design Strategy 2 samples performed very well in this test, ranked as either A or B (zero or one visible scratch), even at the most severe scratching load levels. This performance is dramatically better than standard chemically strengthened glass, which consistently is ranked D (3 or more visible scratches) in this test. These results suggest that the "buried active layers" approach is highly successful both in maximizing surface hardness and minimizing scratch visibility after aggressive scratch testing. Separately selected samples were also tested for environmental/chemical durability through (1) abrading the samples with 400 grit Al_2O_3 sandpaper using 50 reciprocating passes with 1 kg applied load over a 1 cm^2 contact area, then (2) exposing the abraded samples to either (a) pH 2.5 or pH 8.6 artificial perspiration solutions for 7 days at room temperature, or (b) 5% NaCl solution for 7 days at 35 °C. No coating corrosion, delamination,

or other adverse effects of chemical exposure were observed after this extensive abrasion and chemical durability testing.

Table 2. Summary of key coating mechanical properties for Design Strategy 2 coatings.

Sample	Garnet Scratch	Hardness at 100 nm	Hardness at 500 nm
-	Grade	GPa	GPa
WSC–Silver–2–B	1 kg:A 4 kg:A	10.8	17.2
WSC–Blue–2–B	1 kg:A 4 kg:B	14.9	19.9
WSC–Pink–2–B	1 kg:A 4 kg:A	11.8	19.0
WSC–Silver–3–B	1 kg:A 4 kg:A	14.4	19.9
Chemically Strengthened Glass (Ref.)	1 kg:D 4 kg:D	~8 GPa	~8 GPa

4. Discussion

Our wavelength-selective coating design approach incorporates interference layer structures with a thick (~2 micron) hard coating region, antireflective interference layers, and wavelength-selective interference layers. This "modular" design approach allows for flexibility of coating thickness and adjustable placement of the wavelength-selective layers while considering likely application scratch depths and the optical effects of such scratches on the interference layers. The coating design approach and scratch testing employed here were significantly informed by studies of field scratches in used consumer electronics devices showing the majority of scratches to be in the depth range of 0.1–1 micron. The hardness and optical properties of each individual layer material were comparable to those reported in previous studies [16–19]; the primary novelty of the present work was the use of a "modular" design approach, in particular, to enable the buried layers approach of Design Strategy 2, resulting in wavelength-selective coatings with levels of hardness and scratch resistance that represented the first demonstrations of their kind. We are not aware of any other reported wavelength-selective optics achieving scratch resistance levels that are at all comparable to chemically strengthened glass. In the present study, wavelength-selective optics were demonstrated, which not only had comparable scratch resistance to chemically strengthened glass, but dramatically exceeded the scratch resistance performance of typical chemically strengthened glass. The practical relevance of this coating design approach, hardness optimization strategy, and scratch resistance tests have been confirmed in real-world applications using optical hard coatings with similar mechanical properties that have been deployed in the field on millions of consumer electronics devices [16].

In this work, Design Strategy 1 employs buried antireflective layers and exposed wavelength-selective layers, while Design Strategy 2 employs buried wavelength-selective layers together with a single exposed antireflective layer. The antireflective layers serve to control the level of reflectance and transmittance oscillations, as well as provide a unique level of ability to vary the thickness of the thickest hard coating layer while maintaining the optical targets of the design. Wavelength selectivity is demonstrated using visible color bandpass filters, with reflection selectivity as high as 7:1 in the case of sample WSC-Pink-2-B. Sample WSC-Silver-2-B demonstrates the feasibility of narrowband transmission in these hard coating designs, with a FWHM (defined here as the midpoint between the maximum and minimum of transmission) of ~8 nm or ~1.6% of the central wavelength. In separate studies, we have performed modeling sensitivity and manufacturing tolerance analyses of similar multilayer optical hard coatings. While a full description of tolerance is beyond the scope of this paper, generally, we have found that index variations less than 1–2% and film thickness variations less than 3–5% are achievable in manufacturing. These levels of variation have been found to be acceptable in

delivering millions of glass parts coated with multilayer optical hard coatings to consumer electronics customers, with high manufacturing yield. Exact tolerance levels have some dependence on the type of wavelength selectivity and spectral features that are targeted.

Hardness profiles for Design Strategy 1 coatings correlate well with the fraction of high-hardness SiN_x material in the outermost layers above the thickest ~2000 nm hard coat layer, while hardness profiles for Design Strategy 2 coatings correlate well with the thickness of the single outermost antireflective, lower hardness SiO_2 layer coated above the thickest hard coat layer. The number and type of layers buried below the 2000 nm thick hard coat layer have relatively less significance to the measured hardness profiles in the depth ranges analyzed here, which were chosen based on the previously mentioned studies of field scratches in consumer devices. Design Strategy 2 coatings demonstrate very high hardness over extended depth ranges, more than double the hardness of typical chemically strengthened glass. Design Strategy 2 coatings have a nanoindentation hardness of 16–20 GPa over an indentation depth range of 200–800 nm and demonstrate particularly excellent resistance to severe scratch testing. The outermost SiO_2 layer in Design Strategy 2 coatings affects the measured hardness at shallow depths as well as deeper depths due to the fact that the indenter continues to interact with the surface SiO_2 layer even at deeper indentation depths. Both the test indenter and real-world scratching particles typically experience an interaction volume (interacting with multiple layers in the coating stack) during an indent or scratch event. This means that, while a surface SiO_2 layer can lower the measured hardness, a surface SiO_2 layer can also be mechanically supported by the hard coating layer underneath, making the entire system highly resistant to scratches even though the surface layer is composed of a relatively lower hardness material such as SiO_2. While hardness appears to be the dominating factor in the scratch resistance tests we have developed to mimic field scratches from the consumer electronics industry, modulus and H/E ratios may warrant further study for additional damage modes [29].

The highest hardness Design Strategy 2 coatings, samples WSC-Blue-2-B and WSC–Silver-3-B, have hardness values of 14–15 GPa at 100 nm depth and 19–20 GPa at 500 nm depth, respectively. In the range of Design Strategy 2 coatings tested, the somewhat lower hardness of sample WSC-Silver-2-B (11 GPa at 100 nm depth and 17 GPa at 500 nm depth) does not result in a visibly lower performance in aggressive garnet scratch testing. From a real-world use perspective, Design Strategy 2 is preferred for multiple reasons. This "buried active layers" approach not only increases the measured indentation hardness of the coatings but is also designed such that when scratch events do occur, the optical impact of the scratches (e.g., change in targeted optical activity, such as reflectance, wavelength selectivity, or color) in a damaged area is minimized. The buried layers approach is enabled by the "modular" coating design strategy described above. In particular, the inclusion of an anti-reflecting layer or layers adjacent to a thick hard coating layer provides flexibility in the hard coating thickness, control over reflectance and transmittance oscillations, and enables the placement of optically active layers below the hard coating layer while still allowing optical performance targets to be met.

5. Conclusions

In this work, we demonstrated initial feasibility in creating wavelength-selective hard coatings with high hardness and mechanical durability that are substantially higher than that of the chemically strengthened glass on which these coatings are fabricated. Two different design strategies for wavelength-selective coatings were demonstrated, employing varying combinations of antireflective layers, hard coating layers, and wavelength-selective interference layers in a "modular" design approach. Design Strategy 2, utilizing buried wavelength-selective interference layers, delivered the highest hardness responses. We believe that the levels of optical performance shown here, either in terms of wavelength selection efficiency or bandwidth, can be further optimized in hard coatings for specific applications utilizing the illustrated design principles. Future applications may include non-visible spectral filters, such as IR or UV bandpass optics. These results pave the way for new uses of wavelength-selective optics in mechanically demanding applications.

6. Patents

1. Bellman, R.A., Hart, S.D., Koch, K.W., and Paulson, C.A. Low-color scratch-resistant articles with a multilayer optical film. U.S. Patent 9,079,802, 2015.
2. Hart, S.D., Koch, K.W., Paulson, C.A., and Price, J.J. Durable and scratch-resistant anti-reflective articles. U.S. Patent 9,335,444, 2016.
3. Hart, S.D., Koch, K.W., Kosik Williams, C.A., Lin, L., Paulson, C.A., and Price, J.J. Reflective, colored, or color-shifting scratch resistant coatings and articles. U.S. Patent 10,162,084, 2018.

Author Contributions: Conceptualization, K.W.K., L.L., J.J.P., C.A.P., A.M., C.K.W. and S.D.H.; methodology, K.W.K., L.L., J.J.P., C.A.P., B.Z. and S.D.H.; validation, C.-G.K., D.-G.M., S.-Y.O., J.-K.O., B.Z., A.S. and J.J.P.; formal analysis, K.W.K., L.L., S.D.H. and C.-G.K.; investigation, C.-G.K., D.-G.M., S.-Y.O., J.-K.O., B.Z., A.S. and J.J.P.; writing—original draft preparation, S.D.H.; writing—review and editing, S.D.H., C.K.W., C.A.P. and J.-H.O.; visualization, S.D.H.; supervision, J.-H.O., A.M. and C.K.W.; project administration, J.-H.O., A.M. and C.K.W. All authors have read and agreed to the published version of the manuscript.

Funding: This research received no external funding.

Acknowledgments: The authors would like to acknowledge Loretta Moses, Jaymin Amin, Kevin Reiman, Leon Reed, Heather Decker, Nicholas Walker, Sanjay Sinha, Robert Bellman, John Langstrand, Junghun Yun, Jinah Yoo, Heeseon You, Jiman Lee, Eunhae Ji, Bill McKendrick, Hazel Russell, Arnette Brooks, Brandy Fuller, Phyllis Markowski, Josh Jacobs, Jum Kim, Robert Lee, and Odessa Petzold, for their assistance in experiments, analysis, logistical support, and moral support.

Conflicts of Interest: All authors are employees of Corning Incorporated or its wholly-owned subsidiaries, which may choose to market or sell technical products related to the subject matter of this article.

Appendix A

Table A1. Summary of detailed coating designs for samples based on Design Strategy 1. The wavelength-selective interference is generated by optical interference layers 8–12, which are on the air side (user-facing side) of the thickest hard coating layer.

Design			WSC-Red-1	WSC-Pink-1	WSC-Green-1	WSC-Blue-1	WSC-Silver-1
Layer	**Material**	**Refractive Index at 550 nm**	**Thickness (nm)**	**Thickness (nm)**	**Thickness (nm)**	**Thickness (nm)**	**Thickness (nm)**
Substrate	Glass	1.51	N/A	N/A	N/A	N/A	N/A
1	SiO_xNy	1.95	8.6	8.3	8.3	8.1	8.2
2	SiO_2	1.48	52.3	52.5	52.4	51.8	51.7
3	SiO_xN_y	1.95	25.5	25.1	25.0	25.1	24.7
4	SiO_2	1.48	30.3	30.2	30.2	29.9	29.9
5	SiO_xN_y	1.95	44.0	43.9	43.7	43.3	42.8
6	SiO_2	1.48	8.7	8.7	8.8	8.5	8.7
7	SiO_xN_y	1.95	2011	2021	2019	1998	2020
8	SiO_2	1.48	149.2	99.7	271.6	268.9	201.1
9	SiN_x	2.01	92.2	102.9	66.0	58.1	189.2
10	SiO_2	1.48	112.8	61.6	20.6	81.6	87.7
11	SiN_x	2.01	103.3	129.8	112.1	30.4	59.7
12	SiO_2	1.48	24.3	26.9	29.4	25.7	25.3
Medium	Air	1	N/A	N/A	N/A	N/A	N/A

Table A2. Summary of detailed coated designs for Design Strategy 2 sample WSC–Silver–2–B.

Design			**WSC-Silver-2-B**
Layer	**Material**	**Refractive Index at 550 nm**	**Thickness (nm)**
Substrate	Glass	1.51	N/A
1	SiO_xN_y	1.95	107.2
2	SiO_2	1.48	14.8
3	SiO_xN_y	1.95	58.0
4	SiO_2	1.48	24.7
5	SiO_xN_y	1.95	9.9
6	SiO_2	1.48	120.3
7	SiO_xN_y	1.95	58.4
8	SiO_2	1.48	101.7
9	SiO_xN_y	1.95	57.6
10	SiO_2	1.48	83.8
11	SiO_xN_y	1.95	62.9
12	SiO_2	1.48	94.8
13	SiO_xN_y	1.95	145.0
14	SiO_2	1.48	78.6
15	SiO_xN_y	1.95	61.4
16	SiO_2	1.48	151.8
17	SiO_xN_y	1.95	85.3
18	SiO_2	1.48	130.0
19	SiO_xN_y	1.95	98.3
20	SiO_2	1.48	179.5
21	SiO_xN_y	1.95	2005
22	SiO_2	1.48	133.3
Medium	Air	1	N/A

Table A3. Summary of detailed coated designs for Design Strategy 2 samples. The wavelength-selective interference is generated by optical interference layers 1–9, which are buried underneath the thickest hard coating layer 10.

Design			**WSC-Blue-2-B**	**WSC-Pink-2-B**	**WSC-Silver-3-B**
Layer	**Material**	**Refractive Index at 550 nm**	**Thickness (nm)**	**Thickness (nm)**	**Thickness (nm)**
Substrate	Glass	1.51	N/A	N/A	N/A
1	SiO_2	1.48	25.0	25.0	25.0
2	SiN_x	2.01	16.1	106.1	92.2
3	SiO_2	1.48	74.0	120.7	102.7
4	SiN_x	2.01	70.0	88.4	121.2
5	SiO_2	1.48	62.9	123.6	75.1
6	SiN_x	2.01	77.7	93.8	62.8
7	SiO_2	1.48	61.1	127.1	95.0
8	SiN_x	2.01	71.8	100.6	177.1
9	SiO_2	1.48	62.6	134.1	108.5
10	SiN_x	2.01	2029	2035	2026
11	SiO_2	1.48	79.2	106.8	93.8
Medium	Air	1	N/A	N/A	N/A

References

1. Macleod, H.A. *Thin-Film Optical Filters*, 5th ed.; CRC Press: Boca Raton, FL, USA, 2017.
2. Baumeister, P.W. Methods of altering the characteristics of a multilayer stack. *J. Opt. Soc. Am. A* **1962**, *52*, 1149–1152. [CrossRef]
3. Southwell, W.H. Coating design using very thin high-and low-index layers. *Appl. Opt.* **1985**, *24*, 457–460. [CrossRef] [PubMed]
4. Raut, H.K.; Ganesh, V.A.; Nair, A.S.; Ramakrishna, S. Antireflective coatings: A critical, in-depth review. *Energy Environ. Sci.* **2011**, *4*, 3779–3804. [CrossRef]
5. Aiken, D.J. High performance anti-reflection coatings for broadband multi-junction solar cells. *Sol. Energy Mater. Sol. Cells.* **2000**, *64*, 393–404. [CrossRef]
6. Fink, Y.; Winn, J.N.; Fan, S.; Chen, C.; Michel, J.; Joannopoulos, J.D.; Thomas, E.L. A dielectric omnidirectional reflector. *Science* **1998**, *282*, 1679–1682. [CrossRef] [PubMed]
7. Szipöcs, R.; Ferencz, K.; Spielmann, C.; Krausz, F. Chirped multilayer coatings for broadband dispersion control in femtosecond lasers. *Opt. Lett.* **1994**, *19*, 201–203. [CrossRef]
8. Weber, M.F.; Stover, C.A.; Gilbert, L.R.; Nevitt, T.J.; Ouderkirk, A.J. Giant birefringent optics in multilayer polymer mirrors. *Science* **2000**, *287*, 2451–2456. [CrossRef]
9. Beauchamp, W.T.; Tuttle-Hart, T. UV/IR Reflecting Solar Cell Cover. U.S. Patent 5,449,413, 12 September 1995.
10. Lequime, M. Tunable thin film filters: Review and perspectives. In *Advances in Optical Thin Films, Proceedings of the SPIE—Optical Systems Design, St. Etienne, France, 30 September–3 October 2003*; International Society for Optics and Photonics: Bellingham, WA, USA, 2004; Volume 5250, pp. 302–311.
11. Williams, C.; Hong, N.; Julian, M.; Borg, S.; Kim, H.J. Tunable mid-wave infrared Fabry-Perot bandpass filters using phase-change GeSbTe. *Opt. Express* **2020**, *28*, 10583–10594. [CrossRef]
12. Scobey, M.A. Stupik. Stable ultranarrow bandpass filters. In *Optical Thin Films IV: New Developments, Proceedings of SPIE's International Symposium on Optics, Imaging, and Instrumentation, San Diego, CA, USA, 25–27 July 1994*; International Society for Optics and Photonics: Bellingham, WA, USA, 1994; Volume 2262, pp. 37–46.
13. Serényi, M.; Rácz, M.; Lohner, T. Refractive index of sputtered silicon oxynitride layers for antireflection coating. *Vacuum* **2001**, *61*, 245–249. [CrossRef]
14. Wang, Y.; Cheng, X.; Lin, Z.; Zhang, C.; Zhang, F. Optimization of PECVD silicon oxynitride films for anti-reflection coating. *Vacuum* **2003**, *72*, 345–349. [CrossRef]
15. Schneider, J.; Schula, S.; Weinhold, W.P. Characterisation of the scratch resistance of annealed and tempered architectural glass. *Thin Solid Films* **2012**, *520*, 4190–4198. [CrossRef]
16. Paulson, C.A.; Price, J.J.; Koch, K.W.; Kim, C.G.; Oh, J.H.; Lin, L.; Subramanian, A.N.; Zhang, B.; Amin, J.; Mayolet, A.; et al. Industrial-grade anti-reflection coatings with extreme scratch resistance. *Opt. Lett.* **2019**, *44*, 5977–5980. [CrossRef]
17. Koch, K.W.; Hathaway, B.; Kosik Williams, C.; Amin, J.; Mayolet, A.; Aurongzeb, D.; McDonald, J.; Hart, S.D. Antireflection displays with ambient contrast enhancement for extended device battery lifetime and reduced energy consumption. *J. Soc. Inf. Disp.* **2020**, *28*, 801–807. [CrossRef]
18. Wang, J.; Bouchard, J.P.; Hart, G.A.; Oudard, J.F.; Paulson, C.A.; Sachenik, P.A.; Price, J.J. Silicon oxynitride based scratch resistant antireflective coatings. In *Advanced Optics for Defense Applications: UV through LWIR III, SPIE Defense + Security, Orlando, FL, USA, 15–16 April, 2018*; International Society for Optics and Photonics: Bellingham, WA, USA, 2018; Volume 10627, p. 106270G.
19. Paulson, C.A. Scratch-Resistant and Optically Transparent Materials and Articles. U.S. Patent 10,603,870, 31 March 2020.
20. Musil, J.; Baroch, P.; Vlček, J.; Nam, K.H.; Han, J.G. Reactive magnetron sputtering of thin films: Present status and trends. *Thin Solid Films* **2005**, *475*, 208–218. [CrossRef]
21. Sproul, W.D. Very high rate reactive sputtering of TiN, ZrN and HfN. *Thin Solid Films* **1983**, *107*, 141–147. [CrossRef]
22. Shimada, M.; Amazawa, T.; Ono, T.; Matsuo, S.; Oikawa, H. Ultrathin Al_2O_3 and AlN films deposited by reactive sputter using advanced electron cyclotron resonance plasma source. *Vacuum* **2000**, *59*, 727–734. [CrossRef]

23. Lehan, J.P.; Sargent, R.B.; Klinger, R.E. High-rate aluminum oxide deposition by MetaMode^{TM} reactive sputtering. *J. Vac. Sci. Technol. A* **1992**, *10*, 3401–3406. [CrossRef]
24. Rademacher, D.; Zickenrott, T.; Vergöhl, M. Sputtering of dielectric single layers by metallic mode reactive sputtering and conventional reactive sputtering from cylindrical cathodes in a sputter-up configuration. *Thin Solid Films* **2013**, *532*, 98–105. [CrossRef]
25. Oliver, W.C.; Pharr, G.M. An improved technique for determining hardness and elastic modulus using load and displacement sensing indentation experiments. *J. Mater. Res.* **1992**, *7*, 1564–1583. [CrossRef]
26. Oliver, W.C.; Pharr, G.M. Measurement of hardness and elastic modulus by instrumented indentation: Advances in understanding and refinements to methodology. *J. Mater. Res.* **2004**, *19*, 3–20. [CrossRef]
27. Lucas, B.N.; Oliver, W.C.; Swindeman, J.E. The dynamics of depth-sensing, frequency-specific indentation testing. *Mat. Res. Soc. Symp. Proc.* **1998**, *522*, 14. [CrossRef]
28. Bressan, J.D.; Tramontin, A.; Rosa, C. Modeling of nanoindentation of bulk and thin film by finite element method. *Wear* **2005**, *258*, 115–122. [CrossRef]
29. Hassani, S.; Bielawski, M.; Beres, W.; Martinu, L.; Balazinski, M.; Klemberg-Sapieha, J.E. Predictive tools for the design of erosion resistant coatings. *Surf. Coat. Technol.* **2008**, *203*, 204–210. [CrossRef]